This is the peer-reviewed, final accepted version for American Mineralogist, published by the Mineralogical Society of America.
The published version is subject to change. Cite as Authors (Year) Title. American Mineralogist, in press.
DOI: https://doi.org/10.2138/am-2022-8505. http://www.minsocam.org/

Revision 1

First evidence of dmisteinbergite ($CaAl_2Si_2O_8$ polymorph) in high grade metamorphic rocks

Iris Wannhoff[1], Silvio Ferrero[2] , Alessia Borghini[3], Robert Darling[4], Patrick J. O´Brien[3]

[1] Institute of Geological Sciences, Freie Universität Berlin, 12249 Berlin, Germany.

[2] Dipartimento di Scienze Chimiche e Geologiche, Universitá di Cagliari, 09042 Monserrato, Italy.

[3] Institute of Geosciences, University of Potsdam, 14476 Potsdam, Germany.

[4] SUNY College at Cortland, New York 13045, US.

Abstract

We identified dmisteinbergite, the rare trigonal polymorph of $CaAl_2Si_2O_8$, for the first time in high-grade metamorphic rocks. Dmisteinbergite occurs as a crystallization product of silicate melt inclusions (nanogranitoids) in garnet from three host rocks with different protoliths and re-equilibration conditions, i.e., from 1.0 to 4.5 GPa. Raman spectra and compositions of the dmisteinbergite here investigated are overall identical to those of previously characterized artificial and natural dmisteinbergite. In nanogranitoids, this phase coexists with other metastable polymorphs of feldspar (kumdykolite, kokchetavite) and SiO_2 (quartz, cristobalite), recently interpreted as the result of melt undercooling, supersaturation and rapid crystallization of a silicate melt confined in a micrometric pore. Dmisteinbergite formation likely results from a similar process and thus it should be regarded as a kinetically-controlled phase. Moreover, the investigation of dmisteinbergite as well as of other metastable feldspar polymorphs offers new insights into the behavior of natural materials under non-equilibrium conditions.

Introduction

Feldspar is one of the major rock-forming minerals in the Earth´s crust, and in recent years its polymorphs are being recognized more and more in very different geological environments

(Krivovichev, 2020 and references therein). In particular, these polymorphs are being increasingly identified as a characteristic feature of anatectic melt inclusions (MI) (Ferrero and Angel, 2018 and references therein; Ferrero et al., 2021a, b). These MI are crystallized droplets of melt, i.e., nanogranitoids (Cesare et al., 2015), entrapped inside a peritectic phase, most commonly garnet, during its formation, hence they are primary as confirmed by their occurrence as clusters in the host (Cesare et al., 2015).

The focus of this study is on the presence within nanogranitoids of a rare trigonal polymorph of $CaAl_2Si_2O_8$, dmisteinbergite (Zolotarev et al., 2019 and references therein). Dmisteinbergite was first identified in the Chelyabinsk coal basin, Russia, on the surface of charcoal from coal dump fire (Chesnokov et al. 1990). This phase was then found in other extreme geological environments such as in different pseudotachylyte veins from the same location (Nestola et al., 2010; Mittempergher et al., 2014) and in meteorites, inside a refractory igneous Ca-Al-rich inclusion in the Allende meteorite (Ma et al., 2013), or as needle-shaped, porous aggregates in Ca-Al rich inclusions in a CV3 carbonaceous chondrite (NWA 2086 meteorite, Fintor et al., 2014). In the laboratory this phase was first synthesized from an anorthitic melt (Davis and Tuttle, 1951), along with another pseudo-orthorhombic (monoclinic) polymorph of $CaAl_2Si_2O_8$, later on named svyatoslavite (Sokol et al. 1998; Chesnokov et al. 1989). A detailed study of the stability, nucleation and growth kinetics of such phases was provided by Abe et al. (1991), Daniel et al. (1995) and Abe and Sunagawa (1995). Their experiments produced dmisteinbergite from an undercooled anorthitic melt at 1200-1400°C (Abe et al., 1991), and Daniel et al. (1995) obtained similar results by melting a synthetic anorthite glass and then cooling it at different rates. Initially described as having hexagonal structure, recently Zolotarev et al. (2019) determined from single-crystal X-ray diffraction (XRD) and Raman spectroscopy studies that this phase is actually trigonal.

Here we report the first finding and characterization of dmisteinbergite in nanogranitoids in garnet from three locations: (1) lower crustal mafic granulites of Gore Mountain (Adirondacks,

US; Wannhoff, 2020; Ferrero et al., 2021b), (2) high *P* felsic granulites of Mount Klet' (Blanský les Massif, Bohemian Massif, Czech Republic; see Franěk et al., 2006 for details on the geological setting), (3) ultrahigh *P* eclogites of the Saidenbach Reservoir (Erzgebirge, Bohemian Massif, Germany; Borghini, 2019). In all three cases, the host rocks re-equilibrated at high *T* (850°C - 1000°C) and highly variable *P* (1.0 to 4.5 GPa), with garnet (re)crystallizing and trapping droplets of melt. The dmisteinbergite-bearing inclusions were investigated with micro-Raman spectroscopy, electron microprobe analysis (EMPA) and field emission gun scanning electron microscopy (FEG-SEM; see methods in Deposit item).

Results

Our investigation shows that dmisteinbergite is more abundant in the mafic granulites of Gore Mountain (Fig. 1a), where it also forms larger crystals in the inclusions (Fig. 1b, c). Here, dmisteinbergite-bearing inclusions can reach 50 μm in diameter, and have a constant mineral assemblage of kumdykolite, amphibole (pargasite and anthophyllite), quartz or cristobalite, with minor rutile or ilmenite (Ferrero et al., 2021b). In Mount Kleť granulites (Fig. 1d) dmisteinbergite was identified in two inclusions with quartz and kokchetavite (as visible in the Raman map in Figure 1e); phlogopite and graphite are also present in the same inclusion (see Fig. 1 in Deposit Item). Kumdykolite (orthorhombic) and kokchetavite (hexagonal) are polymorphs of $NaAlSi_3O_8$ and $KAlSi_3O_8$ respectively and they are commonly found in nanogranitoids (Ferrero et al., 2016, 2021a, b; Borghini et al., 2018; 2020). Raman spectra were acquired on dmisteinbergite in inclusions exposed on the surface in both Gore Mountain and Mount Kleť samples. The Raman spectra of dmisteinbergite from these two localities are almost identical (Table 1). The spectra show four strong to very strong vibrational bands at 118 cm^{-1}, 329 cm^{-1}, 445 cm^{-1} and 914 cm^{-1}, several weak to medium peaks at 139 cm^{-1}, 223 cm^{-1}, 434 cm^{-1}, 394 cm^{-1}, 507 cm^{-1}, 685 cm^{-1}, 802 cm^{-1}, 897 cm^{-1} and a very small peak at 1124 cm^{-1} (Fig. 1c, f), as well as a shoulder at 650 cm^{-1} (only in Fig. 1c). Dmisteinbergite is clearly distinguishable from other $CaAl_2Si_2O_8$ polymorphs by its main peaks at 118 cm^{-1} and 445 cm^{-1}, whereas the

main peaks of anorthite and svyatoslavite are between 500 and 510 cm^{-1}. The nanogranitoids in the Saidenbach eclogites (Fig. 1g, h) contain instead a more complex phase assemblage: biotite, calcite, kumdykolite/albite, quartz/cristobalite, white mica, kokchetavite ± glass, graphite and rarely dmisteinbergite (Borghini, 2019). The spectrum in Figure 1i is from a small inclusion (<6 μm) below the surface, and thus it also contains peaks of other phases in the inclusion, namely quartz and biotite, and of the host garnet. EMPA analyses show that dmisteinbergite crystals from Gore Mountain and Mount Klet' granulites are both almost pure in An component (Table 2) with very small and variable amounts of K_2O and Na_2O, and may also incorporate small amounts (<1 wt%) of FeO, MgO, TiO_2 and SrO. FeO and MgO occur in similar amounts in both localities from the present work and in the CV3 chondrite (Fintor et al., 2014), whereas the dmisteinbergite of Gore Mountain appears to have the highest amount of TiO_2 (0.19 wt%) and SrO (0.12 wt%) so far reported in this phase.

Features of dmisteinbergite in metamorphic rocks vs previous findings

This study reports the first finding of dmisteinbergite in high grade metamorphic rocks inside former melt inclusions. This phase is interpreted to have crystallized from silicate melts after their entrapment during garnet growth, just like the other phases found in the inclusions (Fig. 1b, e, h; see also Cesare et al., 2015). This inference is supported by the complete re-homogenization of the inclusions to glass when reheated under confining *P* in both Gore Mountain (Ferrero et al., 2021b) and Saidenbach (Borghini, 2019).

The Raman spectra are overall similar to the holotype dmisteinbergite from the Chelyabinsk coal basin (Zolotarev et al., 2019; Fig 1k) and of the meteorite sample NWA 2086 CV3 chondrite (Fintor et al., 2014; Fig 1j), with only minor differences in the intensities and position of certain Raman bands (Table 2; Fig 1c,f,i,j,k). For example, in Zolotarev et al. (2019) the peak at 116 cm^{-1} was described as a weak band, whereas in our study this peak is rather significant and is often the most intense. The peaks at 223 cm^{-1} and 329 cm^{-1} are clearly distinguishable, whereas the latter shows a stronger intensity with respect to the peak at 223 cm^{-1} in this study

and in Fintor et al. (2014). In Zolotarev et al. (2019) these peaks were reported to be weak and strong respectively. The peak at 487 cm^{-1} is missing both in this study and in Fintor et al. (2014), whereas the peak at 503 cm^{-1} (Zolotarev et al., 2019) is here shifted to 506 cm^{-1}. The 503 cm^{-1} peak of garnet does not overlap with the 506 cm^{-1} peak in case of Gore Mountain and Mount Klet' - this was tested by comparing the acquired spectra with that of the host garnet. The peak at 801 cm^{-1} is rather weak in all cases, similarly to what is reported by Fintor et al. (2014). Further bands at 1124 cm^{-1} in the CV3 chondrite sample or at 650 cm^{-1} from Chelyabinsk were previously attributed to nanometer-sized inclusions of quartz or anorthite (Zolotarev et al., 2019). In the present study, these peaks are clear and relatively high in intensity and this observation, coupled with prior reports, may indicate that they are instead a characteristic feature of dmisteinbergite, rather than due to nano-inclusions as previously proposed, in which case smaller peak intensities would be expected. Differences in intensities could be due to different orientations of the investigated crystal with respect to the holotype dmisteinbergite. Another possibility is that such differences may relate to the mechanism of formation of the phase. So far, dmisteinbergite was identified in widely different environments (experiments, crystallization product of a gaseous phase in coal dumps, pseudotachylytes, in meteorites, confined melt), where it was proposed to have crystallized as a result of different processes (e.g., crystallization from a melt or gaseous phase). The Raman spectra of this study and those from the CV3 chondrite (Fintor et al., 2014) are very similar in terms of peak position and intensity. However, the intensities reported for the peaks at 115 cm^{-1}, 327 cm^{-1}, 801 cm^{-1} and 892 cm^{-1} by Zolotarev et al. (2019) seem to be reversed with respect to both our study and Fintor et al. (2014) and closer instead in intensities to the spectrum of synthetic dmisteinbergite from Daniel et al. (1995). Considering that all Raman spectra were acquired from samples which formed within different geological settings or were synthesized, this study suggests that the deviations in the Raman spectra of dmisteinbergite are based on small symmetrical differences of the crystal structure which might be in turn dependent on the formation of the

crystal. Zolotarev et al. (2019) interpreted this observation to be the result of Al/Si ordering to variable degrees equivalent to anorthite (Freeman et al., 2008). In more detail, the most ordered anorthite has a Raman peak at 488 cm^{-1}, which is ascribed to the symmetric bending vibrations of Si-O and Al-O bonds and shifted to 485 cm^{-1} for shocked or HT anorthite (Zolotarev et al., 2019). Applying this to dmisteinbergite, it was therefore proposed that dmisteinbergite from the chondrite (Fintor et al., 2014) is more disordered. As this peak is completely absent also in the spectra collected in our study, it is possible that the dmisteinbergite we investigated is disordered as well. Hence, it appears likely that both a hydrothermal origin and one from melt crystallization in a confined space may lead to the formation of disordered dmisteinbergite, whereas deposition from gas (Chesnokov et al., 1989) or cooling of an anorthitic melt (Daniel et al., 1995) provided a more ideal environment for the formation of ordered dmisteinbergite. This supports the observation of Zolotarev et al. (2019) proposing the existence of several varieties of dmisteinbergite, which was rooted in the identification of symmetrical disorders and polytypic variations.

Dmisteinbergite as a metastable polymorph

The formation of the $CaAl_2Si_2O_8$ polymorph dmisteinbergite rather than the more stable counterpart anorthite was already proposed to be the result of metastable crystallization (Krivovichev et al., 2012; Zolotarev et al., 2019; Krivovichev, 2020) regardless of its occurrence in natural rocks (Ma et al., 2013; Fintor et al., 2014; Nestola et al., 2010) or in experiments (Abe et al., 1991; Abe and Sunagawa, 1995; Daniel et al., 1995; Maeda and Yasumori, 2017). The basis of the crystal structure of the metastable feldspar polymorphs are tetrahedrally coordinated Al^{3+} and Si^{4+} cations as in their stable counterparts, although with major structural differences with respect to the feldspar framework topology (Zolotarev et al., 2019). These observations conform with Goldsmith´s principle of simplexity (Goldsmith, 1953), which states that less complex phases crystallize with less difficulty with respect to more complex phases. This principle is observed during the formation of metastable phases, which

have a simpler structure than their thermodynamically stable counterparts under non-equilibrium conditions, e.g., when the reaction rate is elevated (Krivovichev et al., 2012; Zolotarev et al., 2019). Rapid crystallization supplies non-equilibrium conditions, and was previously interpreted to be the process responsible for the crystallization of dmisteinbergite and svyatoslavite in the coal dumps from Chelyabinsk (Krivovichev et al., 2012) and in experimental setups (Abe et al., 1991). Indeed, rapid crystallization has been already proposed to be commonplace in anatectic MI, in order to explain the presence of metastable kumdykolite, kokchetavite and cristobalite (Ferrero and Angel, 2018). Crystallization is known to be inhibited when a fluid/melt occur in a restricted volume (<5-10 μm) such as an inclusion/pore (Cesare et al., 2015 and references therein), and this may result in supersaturated and undercooled melts, possibly persisting in a liquid form even well below the solidus T of the system (e.g., Lofgren, 1974). Such conditions can be reasonably expected "…to promote rapid crystallization once the process starts" (Ferrero and Angel, 2018), as experimentally verified for pegmatitic melts (Sirbescu et al., 2017). Thus, the coexistence in inclusions of dmisteinbergite with the other metastable polymorphs strongly suggests that all these metastable phases are the result of the same process, i.e., rapid crystallization due to undercooling/supersaturation of the melt. This provides further insights into the behaviour of confined melts. Whereas metastable polymorphs such as kokchetavite and cristobalite were experimentally reproduced at relatively low T, i.e., <650°C (Ferrero et al., 2016 and references therein), in experiments dmisteinbergite is observed to form at *T* well in excess of 1000°C, thus suggesting that it is possible to achieve conditions favourable to metastable crystallization (i.e., undercooling - supersaturation - rapid crystallization) at very high *T*, possibly even during the first phases of melt/rock cooling, when the parental melt is hosted in a micrometric pore.

Implications

Our study provides two novel insights in the formation of dmisteinbergite, the trigonal polymorph of $CaAl_2Si_2O_8$: 1) this phase can be also found in high grade metamorphic rocks,

and 2) it can crystallize directly not only from purely anorthitic melts, but also from silicate melts with compositions from trondhjemitic (Gore Mountain, Ferrero et al., 2021b) to granitic (Saidenbach, Borghini, 2019).

In terms of *P-T* conditions of formations, our work is overall consistent with previous studies. The occurrence of dmisteinbergite in a closed system such as a preserved melt inclusion brackets its crystallization to have occurred below the entrapment *T* of the melt during garnet growth. In the Mount Klet' granulites, phase equilibrium modelling suggests $T \leq 850$°C for garnet formation (Franěk et al., 2006) and thus melt entrapment, whereas Gore Mountain nanogranitoids were originally trapped at ~ 940°C, based on re-homogenization and modelling (Ferrero et al., 2021b). More precise estimates are not possible without further studies on the crystallization behaviour of the trapped melt in micrometric pores. In the Chelyabinsk coal basin it was inferred that dmisteinbergite crystallized from the gas phase at ~ 1000°C (Chesnokov et al., 1990), whereas in pseudotachylite it was inferred to have formed at 1400°C, based on independent estimates (Nestola et al., 2010) and similarities with experiments (Daniels et al., 1995). Similarly, also the crystallization *P* of the phases in the inclusions is bound to be lower than the *P* at which the original melt was trapped. During cooling and crystallization, internal *P* and *T* of the MI follow a precise, almost isochoric path with positive slope (an example is visible in Ferrero et al., 2016). Assuming that the host rock experienced exclusively cooling after garnet formation and melt entrapment at the metamorphic peak (a scenario overall compatible with most trajectories of deeply subducted crustal rocks) and that dmisteinbergite is one of the first phases to crystallize from the melt (consistently with its high formation *T* and analogy to anorthite) our findings support its crystallization over a wide *P* range, from ≤1.6 GPa (Mount Klet', Franěk et al., 2006) to ≤4.5 GPa (Saidenbach, Borghini, 2019). A lower limit for the formation *P* cannot be established to date, but if dmisteinbergite is one of the first phases to crystallize it is likely that the MI only experienced limited depressurization before crystallization commenced. When observations on natural samples are merged with those from

experiments (which were all conducted at atmospheric *P*), it appears self-evident that *P* by itself has no clear influence on dmisteinbergite formation. This is also consistent with the previous studies of dmisteinbergite in meteorites, where this phase is not proposed to have formed during impact, but as result of hydrothermal alteration of the host rock still on the parent asteroid (Fintor et al., 2014). Furthermore, synthetic dmisteinbergite can be formed through water-rock (or cement) interactions at hydrothermal conditions (T ~200-300°C, Pyatina & Sugama, 2020 and references therein). Another natural example supporting that *P* is not influential to the formation of dmisteinbergite is the occurrence of dmisteinbergite inclusions in moissanite, where it formed exsolution lamella (Di Pierro & Gnoss., 2016) interpreted to be the result of moissanite retrogression.

In conclusion, as the investigation of nanogranitoids in metamorphic rocks moves forward, more and more metastable polymorphs are being identified in inclusions that were cooling/depressurizing over an extremely wide *P*-*T* range, i.e., 800°C -1050°C and 0.5–4.5 GPa (Ferrero and Angel, 2018; Ferrero et al., 2021b; this work). When compared with our experiment-based knowledge of such phases, this string of new findings provides definitive proof that feldspar polymorphs can form at any *T* above 500°C (Ferrero et al., 2016) and *P* from atmospheric to the stability field of diamond. In our opinion, all of this evidence makes a compelling case in support of the hypothesis that the formation of metastable polymorphs is controlled by the kinetics of the crystallization process, rather than the establishment of precise *P*-*T* conditions in the inclusion undergoing cooling. Furthermore, our discoveries show that further studies, both experimental and on natural rocks, targeting metastable polymorphs of feldspar are still required to achieve a more complete understanding of the behaviour of natural materials under non-equilibrium conditions.

Acknowledgements

The authors are grateful to C. Günter for assistance during analyses and to C. Fischer for sample preparation. This research was funded by the German Federal Ministry for Education and

234 Research and by the Deutsche Forschungsgemeinschaft (Project FE 1527/2-3 and FE 1527/4-1
235 to S.F). We are thankful to S. Mittempergher and an anonymous reviewer for their thoughtful
236 comments.

237 **References cited**

238 Abe, T., and Sunagawa, I. (1995) Hexagonal $CaAl_2Si_2O_8$ in a high T solution; metastable
239 crystallization and transformation to anorthite. Mineralogical Journal, 17, 257–281.
240 Abe, T., Tsukamoto, K., and Sunagawa, I. (1991) Nucleation, growth and stability of
241 $CaAl_2Si_2O_8$ polymorphs. Physics and Chemistry of Minerals, 17, 473–484.
242 Borghini, A. (2019) Melt inclusions in mafic rocks as witnesses of metasomatism in the
243 Bohemian Massif. PhD thesis, Universität Potsdam, 125 pp.
244 Borghini, A., Ferrero, S., O'Brien, P.J., Laurent, O., Günter, C., and Ziemann, M.A. (2020)
245 Cryptic metasomatic agent measured in situ in Variscan mantle rocks: Melt inclusions in
246 garnet of eclogite, Granulitgebirge, Germany. Journal Metamorphic Geology, 38, 207–234.
247 Borghini, A., Ferrero, S., Wunder, B., Laurent, O., O'Brien, P.J., and Ziemann, M.A. (2018)
248 Granitoid melt inclusions in orogenic peridotite and the origin of garnet clinopyroxenite.
249 Geology, 46(11), 1007–1010.
250 Cesare, B., Acosta-Vigil, A., Bartoli, O., and Ferrero, S. (2015) What can we learn from melt
251 inclusions in migmatites and granulites? Lithos 239, 186–216.
252 Chesnokov, B.V., Lotova, E.V., Nigmatulina, E.N., Pavlyuchenko, V.S., and Bushmakin, A.F.
253 (1990) Dmisteinbergite $CaAl_2Si_2O_8$ (hexagonal)—A new mineral. Zapiski Vsesoyuz
254 Mineralogicheskogo Obshchestva, 119, 43–45.
255 Chesnokov, B.V., Lotova, E.V., Pavlyuchenko, V.S., Nigmatulina, E.N., Usova, L.V.,
256 Bushmakin, A.R., and Nishanbaev, T.P. (1989) Svyatoslavite, $CaAl_2Si_2O_8$ (orthorhombic),
257 a new mineral. Zapiski Vsesoyuz Mineralogicheskogo Obshchestva, 118, 111–114.

Daniel, I., Gillet, P., McMillan, P.F., and Richet, P. (1995) An in-situ high-temperature structural study of stable and metastable $CaAl_2Si_2O_8$ polymorphs. Mineralogical Magazine, 59, 25–33.

Davis, G.L., and Tuttle, O.F. (1951) Two new crystalline phases of the anorthite composition, CaO-Al_2O_3-SiO_2. American Journal of Science. Bowen Volume., 1, 107–114.

Di Pierro, S. and Gnoss, E. (2016) Ca-Al-silicate inclusions in natural moissanite (SiC) American Mineralogist, 101, 71-81, https://doi.org/10.2138/am-2016-5357

Ferrero, S., and Angel, R.J., (2018) Micropetrology: are inclusions in minerals grains of truth? Journal of Petrology, Vol. 59, No. 9, 1671–1700.

Ferrero, S., Ague, J.J., O'Brien, P.J., Wunder, B., Remusat, L., Ziemann, M.A., and Axler, J. (2021a) High pressure, halogen-bearing melt preserved in ultra-high T felsic granulites of the Central Maine Terrane, Connecticut (US). American Mineralogist, 106, 1225–1236.

Ferrero, S., Wannhoff, I., Laurent, O., Yakymchuk, C., Darling, R., Wunder, B., Borghini, A., and O´Brien, P.J. (2021b) Embryos of TTGs in Gore Mountain garnet megacrysts from water-fluxed melting of the lower crust. Earth and Planetary Science Letters, 569, 117058.

Ferrero, S., Ziemann, M.A., Angel, R., O´Brien P.J., Wunder, B. (2016) Kumdykolite, kokchetavite and cristobalite crystallized in nanogranites from felsic granulites, Orlica-Snieznik Dome (Bohemian Massif): not an evidence for ultrahigh pressure conditions. Contributions to Mineralogy and Petrology, 171, 3.

Fintor, K., Park, C., Nagy, S., Pál-Molnár, E., and Krot, A.N. (2014) Hydrothermal origin of hexagonal CaAl2Si2O8 (dmisteinbergite) in a compact type A CAI from the Northwest Africa 2086 CV3 chondrite. Meteoritics & Planetary Science, 201449, 812–823.

Franěk, J., Schulmann, K., and Lexa, O. (2006) Kinematic and rheological model of exhumation of high pressure granulites in the Variscan orogenic root: example of the Blanský les granulite, Bohemian Massif, Czech Republic. Mineralogy and Petrology, 86, 253–276.

Freeman, J.J., Wang, A., Kuebler, K.E., Jolli, B.L., and Haskin, L.A. (2008) Characterization of natural feldspars by Raman spectroscopy for future planetary exploration. The Canadian Mineralogist, 46, 1477–1500.

Goldsmith, J.R., 1953. A "simplexity principle" and its relation to "ease" of crystallization. Journal of Geology, 61, 439–451.

Krivovichev, S.V. (2020) Feldspar polymorphs: diversity, complexity, stability. Proceedings of the Russian Mineralogical Society, 149, 16-66.

Krivovichev, S.V., Shcherbakova, E.P., and Nishanbaev, T.P. (2012) The crystal structure of svyatoslavite and evolution of complexity during crystallization of a $CaAl_2Si_2O_8$ melt: a structural automata description. The Canadian Mineralogist. Vol. 50, 585-592

Lofgren G. (1974) An experimental study of plagioclase crystal morphology: isothermal crystallization. American Journal of Science 274, 243–273.

Ma, C., Krot, A.N., and Bizzarro, M. (2013) Discovery of dmisteinbergite (hexagonal $CaAl_2Si_2O_8$) in the Allende meteorite: A new member of refractory silicates formed in the solar nebula. American Mineralogist, 98, 1368–1371.

Maeda, K., and Yasumori, A. (2017). Nucleation and growth of hexagonal $CaAl_2Si_2O_8$ crystals in $CaO–Al_2O_3–SiO_2$ glass. Material Letters, 206, 241–244.

Mittempergher, S., Dallai, L., Pennacchioni, G., Renard, F., Di Toro, G. (2014) Origin of hydrous fluids at seismogenic depth: Constraints from natural and experimental fault rocks. Earth Planetary Science Letters, 385, 97–109.

Nestola, F., Mittempergher, S., Toro, G.D., Zorzi, F., and Pedron, D. (2010) Evidence of dmisteinbergite (hexagonal form of $CaAl_2Si_2O_8$) in pseudotachylyte: A tool to constrain the thermal history of a seismic event. American Mineralogist, 95, 405–409.

Pyatina, T., Sugama, T. (2020) Cements with supplementary cementitious materials for high-temperature geothermal wells, Geothermics, Volume 86, 101840, https://doi.org/10.1016/j.geothermics.2020.101840.

310 Sirbescu, M. L. C., Schmidt, C., Veksler, I. V., Whittington, A. G., and Wilke, M. (2017)
311 Experimental crystallization of undercooled felsic liquids: generation of pegmatitic texture.
312 Journal of Petrology, 58, 539–568.
313 Sokol, E., Volkova, N., and Lepezin, G. (1998) Mineralogy of pyrometamorphic rocks
314 associated with naturally burned coal-bearing spoil-heaps of the Chelyabinsk coal basin,
315 Russia. European Journal of Mineralogy, 10, 1003–1014.
316 Wannhoff, I. (2020) Melt inclusion investigation reveals first evidence of partial melting in
317 giant garnets of Gore Mountain (Adirondacks, USA). Master thesis, Universität Potsdam.
318 Zolotarev, A.A., Krivovichev, S.V., Panikorovskii, T.L., Gurzhiy, V.V., Bocharov, V.N., and
319 Rassomakhin, M.A. (2019) Dmisteinbergite, $CaAl_2Si_2O_8$, a Metastable Polymorph of
320 Anorthite: Crystal-Structure and Raman Spectroscopic Study of the Holotype Specimen.
321 Minerals, 9, 570.
322 https://rruff.info/Dmisteinbergite/R130085, last accessed 30.06.2022
323

Figures

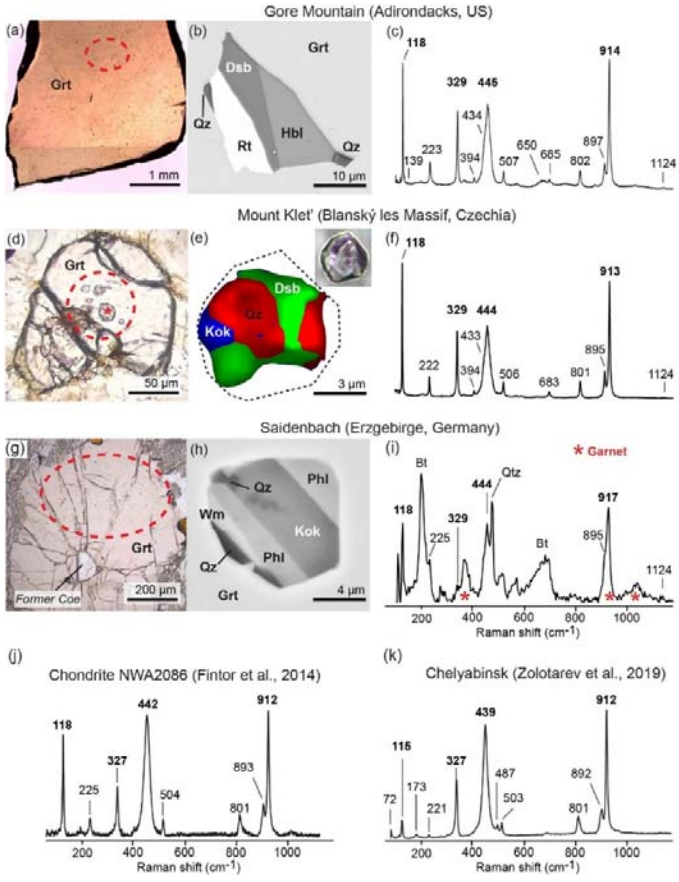

Fig. 1) **(a)** chip of garnet (Grt) from Gore Mountain (Adirondacks); **(b)** Back-Scattered Electron (BSE) image of nanogranitoid. Rt = rutile; Hbl = hornblende; Qz = quartz; Dsb = dmisteinbergite; **(c)** Raman spectrum of Dsb from (b). Main peaks in bold; **(d)** garnet from Mount Klet' (Blanský les Massif,Bohemian Massif). Red star: location spectrum in (f); **(e)** transmitted-light photomicrograph (inset upper right) and Raman map of a nanogranitoid. Color coding: Green = Dsb, peak 118 cm^{-1}, Blue= kokchetavite (Kok), peak 392 cm^{-1}, Red= Qz, peak 464 cm^{-1}; **(f)** Raman spectrum of Dsb from (d). **(g)** Garnet from Saidenbach UHP eclogites (Erzgebirge, Bohemian Massif). Coe = Coesite. Dashed red circles: cluster of nanogranitoids; **(h)** nanogranitoid, BSE image. Wm = white mica; Phl = phlogopite; **(i)** mixed Raman spectrum containing dmisteinbergite, biotite (Bt) and quartz. (j) published spectrum of Dmisteinbergite from (source: https://rruff.info/Dmisteinbergite/R130085) and (k) A. Zolotarev (pers.comm)

This is the peer-reviewed, final accepted version for American Mineralogist, published by the Mineralogical Society of America.
The published version is subject to change. Cite as Authors (Year) Title. American Mineralogist, in press.
DOI: https://doi.org/10.2138/am-2022-8505. http://www.minsocam.org/

Table 1 Reported Raman peaks for dmisteinbergite

Daniel et al. 1995	Fintor et al. 2014	Zolotarev et al. 2019	Gore Mountain	Mount Kletˊ this study	Saidenbach
synthetic	meteorite	coal basin	MI in granulite	MI in granulite	MI in eclogite
77	weak	72 w	/	/	/
96	/	/	/	/	/
120 m	/	115 w	118 vs	118 vs	121 m
133 s	/	/	123 vw	123 vw	/
141 sh	/	/	139 w	139 vw	/
168 m	/	173 w	/	/	/
197 sh	/	/	/	/	/
225 m	/	221 w	223 m	222 m	226 m
303 sh	/	/	/	/	/
329 s	327 m	327 s	329 s	329 s	331 w
/	/	/	394 w	394 w	
419 sh	/	/	434 sh	433 sh	435 sh
445 vs	442 s	439 s	445 s	444 s	447 s
486 m	/	487 s	/	/	/
507 w	504 w	503 w	507 m	506 m	507 m
574 w	/	/	650 sh	/	/
685 m	/	/	685 w	683 w	685 m
809 s	801 w	801 s	802 m	801 m	
899 sh	893 sh	892 s	897 m	895 m	901 sh
916 s	912 s	912 s	914 vs	913 vs	916 s
944 sh	/	/	/	/	/
994 w	/	/	/	/	/
1128 w	/	/	1124 vw	1124 vw	1124 vw

Table 1) Measured and reported Raman peaks for dmisteinbergite. vw = very weak; w = weak; m = medium, s = strong; vs = very strong; sh = shoulder.

Table 2 Electron microprobe analyses of dmisteinbergite

wt%	This work				Sokol et al. (1998)	Fintor et al. (2014)	Ma et al. (2013)
Sample	Gore Mountain		Mount Kletˊ		Pyromet.	CV3	Allende
	av. N=3	std. dev.	av. N=3	std. dev.	Rocks	chondrite	meteorite
SiO_2	42.79	0.15	44.71	0.81	43.89	41.80	42.60
TiO_2	0.19	0.04	0.01	0.01	n.d.	0.04	n.d.
Al_2O_3	36.57	0.31	35.71	0.35	35.39	36.80	36.90
FeO	0.87	0.05	0.95	0.03	0.01	0.54	n.d.
MnO	0.02	0.02	0.02	0.01	0.00	0.04	n.d.
MgO	0.18	0.14	0.12	0.03	0.01	0.61	0.05
CaO	19.91	0.12	19.37	0.17	19.29	19.10	20.20
Na_2O	0.06	0.04	0.05	0.02	0.32	0.19	0.00
K_2O	0.00	0.00	0.15	0.03	0.03	0.03	n.d.
SrO	0.12	0.02	0.01	0.01	n.d.	n.d.	n.d.
BaO	0.01	0.01	0.00	0.01	n.d.	n.d.	n.d.
Total	100.73	0.06	101.11	0.30	98.94	99.15	99.75
No. of oxyger	8.00	8.00	8.00	8.00	8.00	8.00	8.00
Si	1.979	0.007	2.050	0.027	2.050	1.960	1.980
Ti	0.007	0.001	0.000	0.000	n.d.	0.002	0.000
Al	1.993	0.017	1.930	0.028	1.950	2.021	2.021
Fe^{2+}	0.053	0.029	0.036	0.001	0.000	0.021	0.000
Mn	0.001	0.001	0.001	0.000	0.000	0.001	0.000
Mg	0.012	0.009	0.008	0.002	0.000	0.043	0.003
Ca	0.986	0.006	0.952	0.013	0.970	0.956	1.006
Na	0.005	0.004	0.004	0.002	0.030	0.017	0.000
K	0.000	0.000	0.009	0.002	0.000	0.002	0.000
Ba	0.000	0.000	0.000	0.000	n.d.	n.d.	n.d.
Sr	0.003	0.001	0.000	0.000	n.d.	n.d.	n.d.
Total	5.021	0.002	4.991	0.012	5.000	5.023	5.010
Ab%	1		0		2.91	1.77	0.00
An%	99		99		96.91	98.05	100.00
Or%	0		1		0.18	0.18	0.00

Table 2) Electron microprobe analyses of dmisteinbergite. n.d.=not determined.